ANL/CMT/CP-100890

In Situ XAFS of The $Li_xNi_{0.8}Co_{0.2}$ Cathode for Lithium-Ion Batteries*

J. Kropf and C. S. Johnson
Chemical Technology Division
Argonne National Laboratory
9700 South Cass Avenue
Argonne, IL 60439

December 1999

To be submitted to the Journal of Material Research

*This work was performed under the auspices of the U.S. Department of Energy, Office of Basic Energy Science/Division of Chemical Science's Electrochemical Energy Storage and Conversion Program under Contract No. W-31-109-ENG-38. Use of the Advanced Photon Source was supported by the U.S. Department of Energy, Basic Energy Sciences, Office of Science (DOE-BES-SC), under Contract No. W-31-109-ENG-38. The MRCAT is funded by the member institutions and DOE-BES-SC under contracts DE-FG02-94ER45525 and DE-FG02-96ER45589.

IN SITU XAFS OF THE $Li_xNi_{0.8}Co_{0.2}O_2$ CATHODE FOR LITHIUM-ION BATTERIES

A. J. Kropf and C. S. Johnson
Argonne National Laboratory, Chemical Technology Division, 9700 South Cass Avenue, Argonne, IL, 60439

ABSTRACT

The layered $LiNi_{0.8}Co_{0.2}O_2$ system is being considered as a new cathode material for the lithium-ion battery. Compared with $LiCoO_2$, the standard cathode formulation, it possesses improved electrochemical performance at a projected lower cost. *In situ* x-ray absorption fine-structure spectroscopy (XAFS) measurements were conducted on a cell cycled at a moderate rate and normal Li-ion operating voltages (3.0-4.1 V). The XAFS data collected at the Ni and Co edges approximately every 30 min. revealed details about the response of the cathode to Li insertion and extraction. These measurements on the $Li_xNi_{0.8}Co_{0.2}O_2$ cathode ($0.29<x<0.78$) demonstrated the excellent reversibility of the cathode's short-range structure. However, the Co and Ni atoms behaved differently in response to Li insertion. This study corroborates previous work that explains the XAFS of the Ni atoms in terms of a Ni^{3+} Jahn-Teller ion. An analysis of the metal-metal distances suggests, contrary to a qualitative analysis of the x-ray absorption near-edge structure (XANES), that the Co^{3+} is oxidized to the maximum extent possible (within the Li content range of this experiment) at $x = 0.47 \pm 0.04$, and further oxidation occurs at the Ni site.

INTRODUCTION

The emergence of portable telecommunications, computer equipment, and ultimately electric vehicles has created a substantial need for improvements in energy storage devices, namely, less expensive batteries that operate for a longer time, are smaller in size, and weigh less. The Li-ion battery possesses the highest energy density of all rechargeable batteries available in the marketplace today, yet there is still an array of new materials that are being developed for the Li-ion battery. These new compounds require further investigation and physical/chemical characterization.

The Li-ion cathode material of choice is $Li_{1-x}CoO_2$, a hexagonally (space group R3m) layered oxide material that, when coupled with a graphite or coke anode (Li_xC_6) and a 1 *M* $LiPF_6$ electrolyte salt in an organic solvent, makes up a Li-ion cell. This battery operates at 4.0 V and has excellent cyclability and long life, but suffers from too low specific capacity [1]. The similar $Li_{1-x}Ni_xO_2$ suffers from a lower rate capability. The rate problem has been associated with Ni migration into sites within the depleted Li layer for $x \leq 0.5$, which causes a deleterious change in the cathode structure [2]. Cobalt has been substituted into the Ni structure to improve the stability of the cathode. Reasons for the improved electrochemical performance accompanying this substitution are not well understood from a structural standpoint.

Significant work has been performed in the area of in situ analysis using x-ray absorption fine-structure spectroscopy (XAFS) and x-ray diffraction (XRD) on materials in the NiO_2 and CoO_2 families [3-9]. These two methods are complementary. *In situ* XRD gives one a good picture of the long-range structural changes in the cathode, but *in situ* XAFS can provide an understanding of the oxidation state as well as short-range ordering, which may not be accessible from XRD. A more detailed examination of the structure of the $Li_xNi_{0.8}Co_{0.2}O_2$ cathode with XAFS during the battery charge cycle can be illuminating in its own right, but also provides an

DISCLAIMER

excellent baseline for further studies in which the cathode material is modified by the introduction of additional elements.

EXPERIMENT

Battery (pouch cell) Construction

The pouch-type battery cell used in this work was assembled and sealed in a helium-atmosphere glovebox. Cathode laminates of nominal composition $LiNi_{0.8}Co_{0.2}O_2$ (Sumitomo Metal and Mining Co., Ltd.) were dried at 80°C in a vacuum oven inside the glovebox prior to assembly. All cell leads and separator materials were rigorously dried in a like manner. The pouch material was a heat-sealable (0.0045-in. thick), transparent, polyester film laminate. The pouch cells are limited by the cathode capacity and contain metallic lithium foil (0.008 in.) as the anode. The electrode configuration featured in these cells uses metallic lithium as the anode on either side of the cathode. This design ensures an excellent current distribution throughout the cell and provides low resistance for improved electrochemistry. Lithium disks (5/8-in. diameter) were punched from the foil, then cold pressed onto copper mesh (5/8-in. diameter) with an arm as the electrode lead. The cathode composite was painted onto a Ni mesh (5/8-in. diameter) from an N-methyl pyrrolidone slurry of 74% active oxide material, 18% graphite, and 8% polyvinyl difluoride. The mesh laminate electrode was first dried in the glovebox at room temperature, then further vacuum dried at 80°C before final assembly. The separator material was Celgard 2400, and it was placed on either side of the cathode mesh. Electrolyte [10] was added to the pouch cell, then a slight vacuum was applied to the cell to pull all air bubbles out of the pouch prior to final sealing. During the XAFS analysis, pressure was applied to the exterior of the pouch to maintain the stability of the electrode assembly.

The cycling of the pouch cell mimicked that of a coin cell. The cathode delivered 195 mAh/g capacity during its first charge, and after the first discharge, the cell was subjected to x-ray absorption analysis during its next full cycle, which was carried out at a C/5 rate (I=0.875 mA/cm^2) between 4.1 and 3.0 V vs. Li (Figure 1). The capacity in the second cycle was 134 mAh/g and 120 mAh/g, respectively, in C2 and D2. This corresponds to the cathode cycling approximately 0.5 Li into and out of its structure. After the run, the cycling curve was matched with the corresponding XAFS spectra.

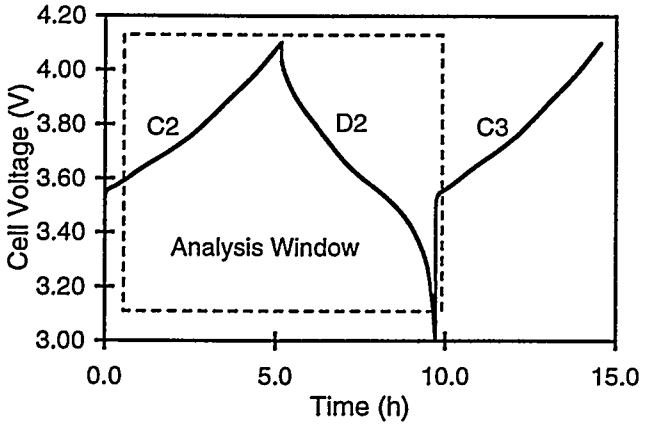

Figure 1. Galvanostatic cycling curve of Li/electrolyte/$Li_xNi_{0.8}Co_{0.2}O_2$ cell during XAFS analysis.

XAFS Measurements

The XAFS measurements were performed on the insertion device (undulator A) beamline of the Materials Research Collaborative Access Team (MRCAT) at the Advanced Photon Source (APS). Using a cryogenically cooled Si(111) double-crystal monochromator, we determined the energy resolution of the monochromatic beam to be ~1.0 eV, as measured by the rocking curve width of the second crystal. An active feedback loop maintained the peak reflectivity of the monochromator, and the resulting large

harmonic content in the beam was rejected by means of a platinum-coated mirror. Transmission ion chambers were used to measure the incident (I_0), transmitted (I_t), and reference (I_{ref}) signals. The I_0 chamber was filled with a helium/nitrogen mixture (50%/50%), while the I_t and I_{ref} chambers were filled with a nitrogen/argon mixture (80%/20%). A beam size of 0.5 x 0.5 mm was chosen in order for the beam to pass easily through the Ni mesh on which the cathode was deposited, resulting in an incident beam flux of ~10^{11} photons/sec. Nickel and Co metal foils were used to calibrate the energy at each edge.

The undulator gap was tapered and the energy range was set to optimize the flux for the Co and Ni edges individually. The monochromator was step-scanned with an integration time of 0.5-2 sec per data point. Including the time spent moving between data points, each scan required about 12 min, corresponding to $\Delta x = 0.021$ ($Li_xNi_{0.8}Co_{0.2}O_2$) from the start to the finish of each scan. The data range at the Co K edge was limited to about 12.5 $Å^{-1}$ by the onset of the Ni K edge. The scan range at the Ni edge was chosen to match the usable range at the Co edge. Spectra were collected alternately at each absorption edge.

DATA ANALYSIS

For the x-ray absorption near-edge spectroscopy (XANES), we calibrated each scan using the appropriate metal foil reference scan taken simultaneously with the battery cell data. The calibration procedure was a qualitative best matching of the entire near-edge region of the reference foil scan to one scan in the battery cell series chosen as the baseline. Even though the energy resolution of the x-ray beam was about 1.0 eV, and the step size in the edge region was only 0.5 eV, shifts as small as 0.1 eV were reliably detected by this calibration method. Absolute energy calibration was made to the Co foil reference scan, assigning an energy of 7709 eV to the maximum derivative. The near-edge regions of selected spectra are shown in Figure 2.

In the XAFS analysis, the FEFF program (version 7.0) [11] was employed for theoretical calculation of the scattering paths, and the FEFFIT program [12] was employed for non-linear least-squares fitting the Fourier Transform (FT) of the XAFS data. In all cases, the Li contribution to the XAFS was ignored.

As mentioned above, the data range limit for both Ni and Co is about 12.5 $Å^{-1}$. The XAFS measurements of the powdered cathode material (*ex situ*, over a longer range), as well as

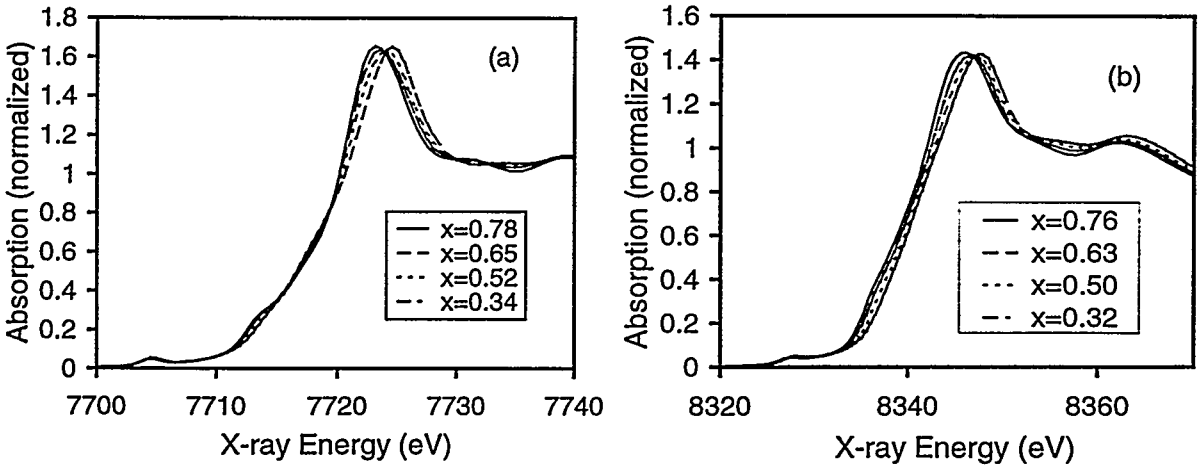

Figure 2. Calibrated and normalized XANES data at the (a) Co and (b) Ni K edges. Reproducibility of the calibration is ±0.1 eV.

literature references [5,7], have shown that the XAFS signal is still strong as far out as 18 $Å^{-1}$. Nonetheless, most analyses of similar materials in the past have limited the upper end of the fitting range to 13-15 $Å^{-1}$. The upper limit of the data range used in this discussion is slightly lower; however, it is adequate for the conclusions presented.

It is not possible to resolve two similar paths with distances separated by less than $\Delta R = \pi/2\Delta k$. For the data range in this study, $\Delta R > 0.16$ Å could theoretically be resolved. Previous measurements of the Jahn-Teller distortion of the NiO_6 octahedron place the effect at about 0.17 ± 0.03 Å [3,4,6,7,9]. This difference is at the limit of the experimental resolution. As a consequence, we used only one Ni-O path to model the NiO_6 octahedron and relied on secondary indicators (i.e., changes in R and σ^2) to reveal the effects of a Jahn-Teller distortion. Trial model optimizations, including both a long and a short Ni-O bond, demonstrated that adding the long-length Ni-O path improved the data fit, but the improvement was not statistically significant.

A third path has been included in the model: the second nearest metal-oxygen (M-O) path at about 3.4 Å. This path overlaps the M-M path due to the phase-shift difference. Including this path in the fit significantly improves the model. The R-factor, a measure of the difference between the data and the model, is between 0.002 and 0.007 [12]. Values for the R-factor that are less than 0.02 generally indicate a good fit.

RESULTS

Unlike pure $LiNiO_2$ or $LiCoO_2$, $Li_xNi_{0.8}Co_{0.2}O_2$ has a hexagonally layered structure that may not undergo phase changes to inactive secondary monoclinic or hexagonal phases when Li is cycled into and out of its lattice. This effect was shown with previous XRD data collected from an *in situ* coin cell [1,8]. In $Li_xNi_{0.8}Co_{0.2}O_2$, it has been postulated that the Ni and Co interlayer slab has a higher degree of covalency; consequently, the Ni-O and Co-O bond strengths are greater than that for the undoped parent materials [2]. The $LiNi_{0.8}Co_{0.2}O_2$ structure thus does not undergo the phase change to monoclinic symmetry, and its ability to cycle Li into and out of the Li layer within the hexagonal (R3m) structure is unimpeded.

The Ni-O and Co-O bond lengths both contract as the Li is removed from the structure during charging (scan numbers 0-23). Both the Co and the Ni become oxidized during this process, each going from a nominal oxidation state of 3^+ to 4^+. During discharge (scan numbers 24-44), this process is reversed electrochemically: Li is reinserted in the lattice structure, the Ni^{4+} and Co^{4+} are reduced to their trivalent states, and their bonds with oxygen return to their original lengths. To a large degree, all of the structural changes visible in the XAFS during the charge are reversed during the discharge. Therefore, in several cases, only data taken during the charge are presented.

XANES

Figures 2(a) and 2(b) show the near-edge regions for selected scans at the Co and Ni edges, respectively. The qualitative difference is immediately apparent. The Ni scans show a steady progression of the entire pattern from lower to higher energy as a function of decreased Li content, indicating an increased average Ni oxidation state, whereas the Co spectra do not follow this progression. Indeed, the shape of the Co absorption spectrum changes markedly from the lower to the higher oxidation state. In both cases, a detailed look at the derivative of the edge spectra reveals that more than a simple edge shift is occurring. Figure 3 is a plot of the white line peak position as a function of the scan number. The cell current changes from lithium extraction (oxidizing) to lithium insertion (reducing) during scan number 23, slightly earlier than

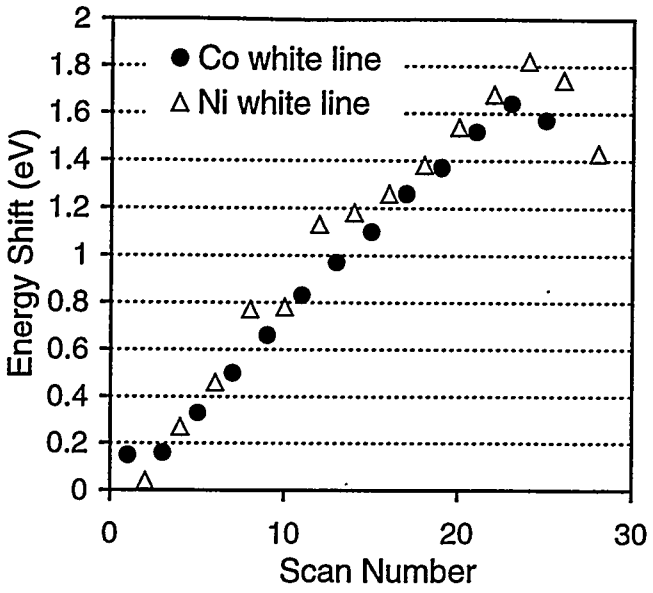

Figure 3. Plot of the white line energy shift versus the scan number. Errors are ±0.1 eV.

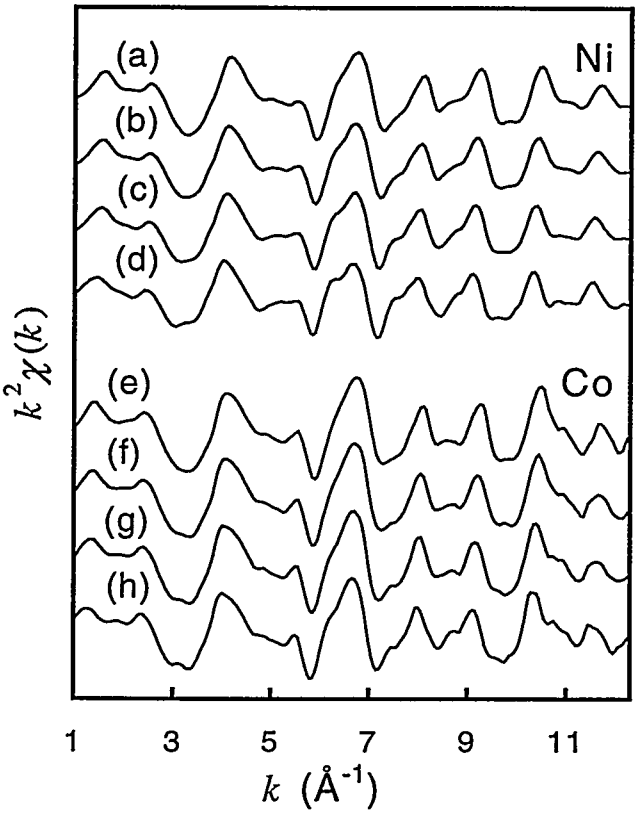

Figure 4. Selected $k^2\chi(k)$ data for Ni and Co; (a) Ni edge, x = 0.32, (b) Ni edge, x = 0.50, (c) Ni edge, x = 0.63, (d) Ni edge, x = 0.76, (e) Co edge, x = 0.34, (f) Co edge, x = 0.52, (g) Co edge, x = 0.65, (h) Co edge, x = 0.78.

the white-line position reverses direction for both Co and Ni. This could be evidence for diffusion of the Li ions into the electrode due to the high charge rate. For both metal centers, the change in the peak position is about +1.7 eV as the lithium content changes from x = 0.78 to x = 0.29.

For the Co edge, two other common measures of the edge position, the energy at normalized μx = 0.5 and the inflection point (maximum of the first derivative), do not follow the change in Li content. However, for the Ni edge, the energy at $\mu x = 0.5$ closely follows the trend of Li insertion. On the other hand, the position of the inflection point can be ambiguous. Therefore, for the Ni edge it is possible to say with a high degree of confidence that the oxidation state is changing smoothly and nearly proportionally to the change in Li content. For the Co edge, the situation is not as clear since the common qualitative indicators contradict each other. To determine the behavior of the Co oxidation, it is useful to turn to the XAFS data.

XAFS

Figure 4 shows normalized $k^2\chi(k)$ data for selected scans throughout the range of x values for both Ni and Co. Only subtle changes take place between x = 0.32 and x = 0.79. Figure 5 shows the FT of the endpoint data. As has been observed previously by Nakai and Nakagome [5], the CoO_6 coordination changes very little with Li content (from an inspection of the FT data). On the other hand, the NiO_6 octahedron changes significantly from one end of the cycle to the other. This has been cited as evidence that Ni^{3+} in these systems is behaving as a Jahn-

Teller ion (octahedral, low-spin d^7 configuration). Longer-range XAFS data, for which the radial distance resolution is high enough to distinguish two oxygen distances, have been used by Pickering, et. al. [4] and Rougier, et. al. [9] to demonstrate the existence of a short and long oxygen bond in the $Li_xNi_{1-x}O_2$ material without Co. In our work, the data have been fit quite well with one Ni-O distance (Figure 6). Qualitatively, it is obvious that the Ni-O shell has a reduced amplitude in the high-x region of the cycle, especially compared with the Co-O shell, which exhibits almost no change. The results of the fits are shown in Table 1.

Two supplementary pieces of evidence suggest the existence of two Ni-O bonds in the Ni^{3+} state. First, when one Ni-O path is used to model the data, the Debye-Waller factor for the oxygen shell decreases and approaches the value for the Co-O path as the Li content decreases. This finding indicates smaller disorder in the bond distance for the Ni^{4+} ion. Second, the Co-O distance changes less than the Ni-O distance, although both exhibit a change essentially proportional to the change in Li content. Figure 7(a) plots the metal-oxygen distance as a function of scan number, while Figure 7(b) plots the difference between the Ni-O and Co-O bond lengths. An explanation for this behavior would be the presence of a long Ni-O bond in the Ni^{3+} octahedron, which reverts to a short bond as Ni^{3+} is oxidized to Ni^{4+}.

The metal-metal neighbor results are key to understanding the difference between the Co and Ni atoms in the cathode. For the sake of simplicity, the second shell around both the Co and the Ni atoms has been modeled as a nickel atom. Practically, this makes very little difference as the back-scattering amplitudes and phase shifts of neighboring elements are virtually indistinguishable. In addition, since the ratio of Ni to Co atoms is 4:1, if the Co and Ni are randomly distributed, there will be 4 to 5 Ni atoms and only 1 to 2 Co atoms in the second shell around each metal atom. As was mentioned earlier, the lithium second-nearest neighbors are neglected. For these reasons and because of the strength of the metal-metal scattering path, it is possible to obtain very precise distances for the metal-metal interaction.

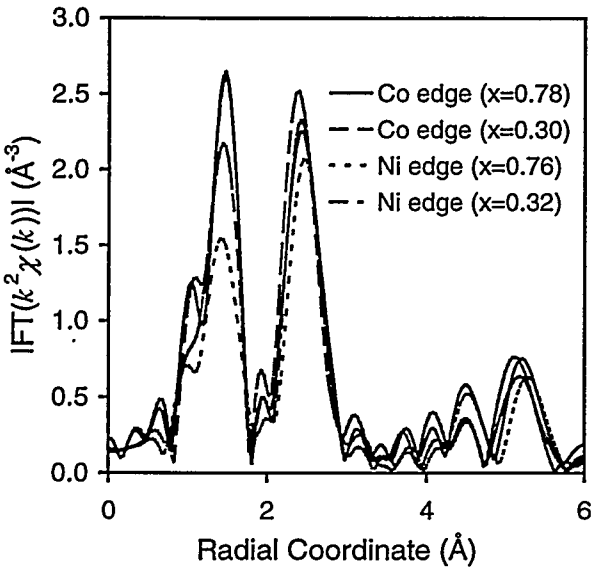

Figure 5. $|FT(k^2\chi(k))|$ of the Co and Ni XAFS at either end of charge cycle. (k-range = 2.0-12.25 Å, modified Hanning window function with $dk = 0.5$ Å^{-1})

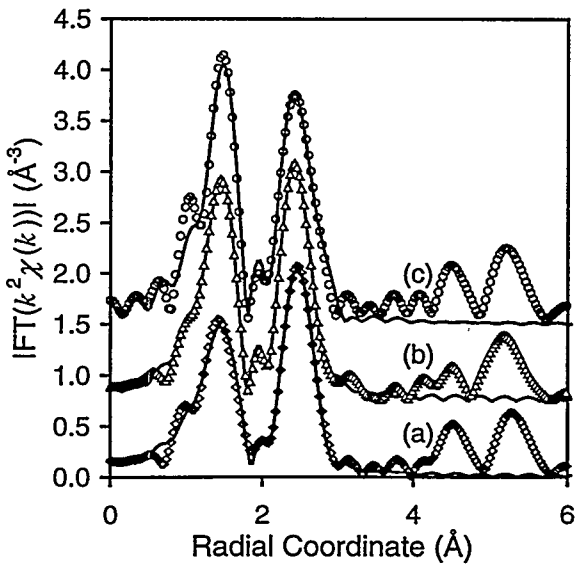

Figure 6. Fit to (a) Co edge, x = 0.78, (b) Ni edge, x = 0.32, and (c) Ni edge, x = 0.76 for scans 1, 2, and 22 (k-range = 2.0-12.25 Å, $dk = 0.5$ Å^{-1}, R-range = 1.1-3.1 Å). The symbols represent the data and the solid lines represent the fit.

Table 1. Fit parameters for the Co and Ni edges (k-range = 2.5 – 11.75 Å^{-1}, dk = 0.5 Å^{-1}, R-range = 1.1 – 3.1 Å). Although 0.0001 Å accuracy is clearly not reasonable for EXAFS (actually 0.02 Å and 0.015 Å for $R_{M\text{-}O}$ and $R_{M\text{-}M}$, respectively), the precision is much greater (0.003 Å and 0.001 Å for $R_{M\text{-}O}$ and $R_{M\text{-}M}$, respectively) given that all systematic errors cancel since it is an identical region of the sample that is measured during each scan. Rounding to 0.001 Å would easily be noticed on the difference plots. Errors for the Debye-Waller factor are 0.4 x 10^{-3} Å^2. Fit parameters for the Ni-O next-nearest-neighbor path are not shown.

Scan # Co Edge	x	$R_{M\text{-}O}$ (Å)	σ^2 (x10^{-3} Å^2)	$R_{M\text{-}M}$ (Å)	σ^2 (x10^{-3} Å^2)	White Line Position (eV)
1	0.78	1.9184	0.8	2.8651	5.4	7728.65
3	0.74	1.9180	0.6	2.8598	5.1	7728.66
5	0.70	1.9156	1.0	2.8555	4.8	7728.83
7	0.65	1.9141	1.2	2.8499	5.1	7729.00
9	0.61	1.9109	1.4	2.8455	4.8	7729.16
11	0.57	1.9063	1.5	2.8430	5.1	7729.33
13	0.52	1.9059	1.3	2.8379	4.7	7729.47
15	0.47	1.9060	1.4	2.8376	4.7	7729.60
17	0.42	1.9051	1.8	2.8344	4.2	7729.76
19	0.38	1.9021	1.4	2.8326	3.5	7729.87
21	0.34	1.9013	1.1	2.8309	3.6	7730.02
23	0.30	1.8982	1.4	2.8287	3.9	7730.14
Ni Edge						
2	0.76	1.9280	6.3	2.8675	4.5	8351.54
4	0.72	1.9203	5.6	2.8637	4.5	8351.77
6	0.68	1.9169	5.5	2.8585	4.7	8351.97
8	0.63	1.9112	5.1	2.8544	4.4	8352.27
10	0.59	1.9079	4.7	2.8509	4.4	8352.28
12	0.55	1.9032	4.4	2.8467	4.3	8352.63
14	0.50	1.9001	3.7	2.8449	4.3	8352.68
16	0.45	1.8956	3.3	2.8410	4.3	8352.76
18	0.40	1.8941	2.9	2.8381	4.4	8352.88
20	0.36	1.8915	2.8	2.8343	4.3	8353.04
22	0.32	1.8898	2.4	2.8309	4.0	8353.18
24	0.31	1.8900	2.6	2.8319	4.1	8353.32

Figure 8(a) plots the M-M distances versus the scan number. There is nearly a 0.04 Å change in $R_{M\text{-}M}$ from x = 0.78 to 0.29 for both the Co and Ni atoms: about a 1.4% linear contraction. However, closer examination reveals that these distances do not change in precisely the same way. The Ni-M distance changes linearly with Li content, while the Co-M bond exhibits two regions. Figure 8(b) shows the difference between $R_{Ni\text{-}M}$ and $R_{Co\text{-}M}$. Between scans 14 and 16 (x = 0.47 ± 0.04) $R_{Co\text{-}M}$ begins to change at a lower rate than $R_{Ni\text{-}M}$. We attribute this difference to the Co atoms being essentially oxidized at this point. The remaining decrease in $R_{Co\text{-}M}$ is due to the secondary effect of the shrinking of the surrounding NiO_6 octahedrons.

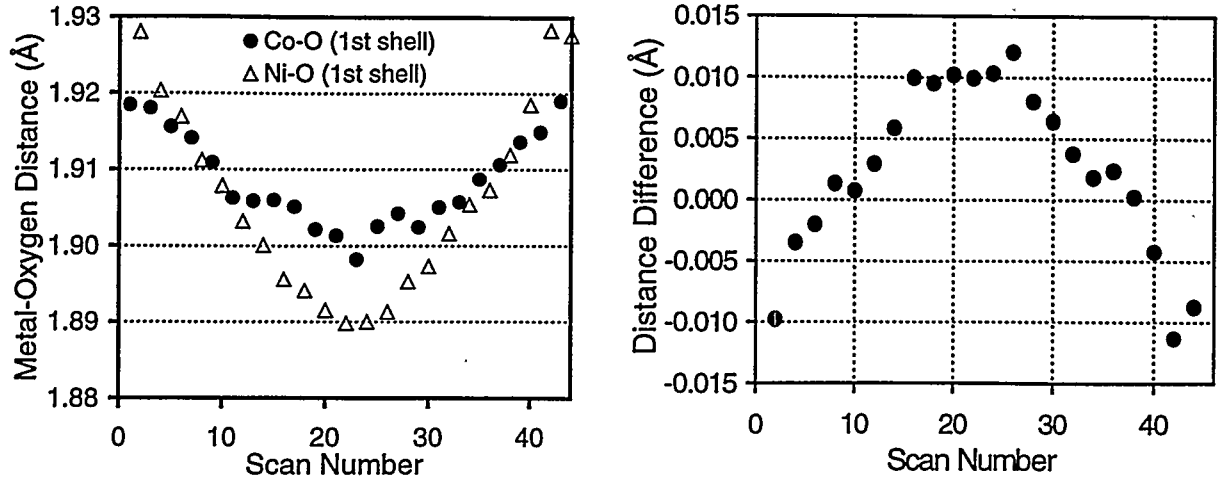

Figure 7. (a) First-shell bond length changes during $Li/Li_xNi_{0.8}Co_{0.2}O_2$ cell cycling (accuracy, ± 0.02 Å, precision, ± 0.003 Å). (b) Difference between $R_{Co\text{-}O}$ and $R_{Ni\text{-}O}$ (± 0.005 Å).

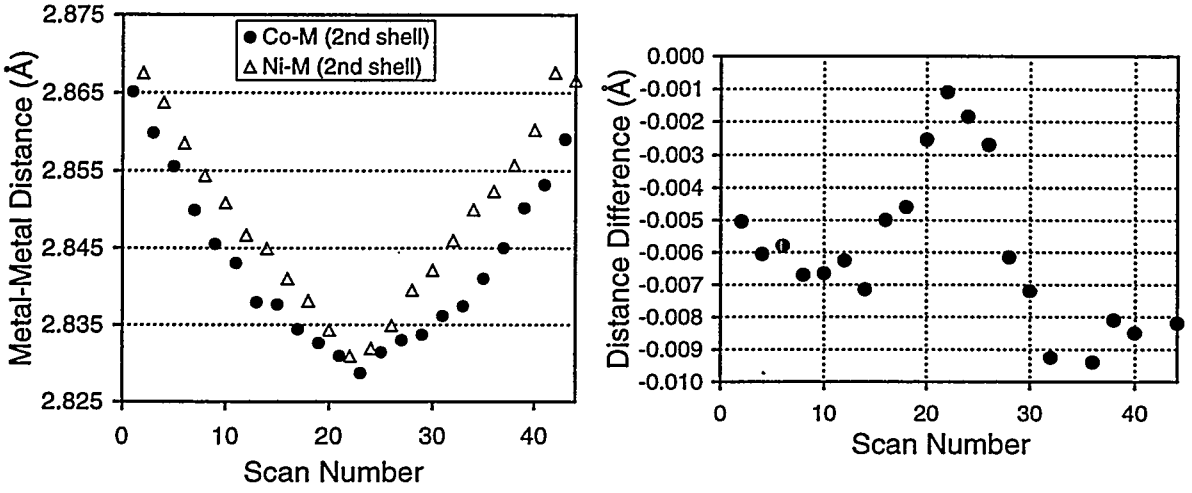

Figure 8. (a) Second-shell metal-metal bond length vs. scan number (accuracy, ± 0.015 Å, precision, ±0.001 Å). (b) Difference between $R_{Co\text{-}M}$ and $R_{Ni\text{-}M}$ (± 0.0015 Å).

CONCLUSIONS

XAFS has provided us with an excellent tool for analyzing the changes that occur when Li is cycled into and out of the layered lattice of $Li_xNi_{0.8}Co_{0.2}O_2$ in a Li-ion battery. This material possesses very desirable characteristics for an electrode, such as small volumetric changes and retention of its structure (on charge and discharge), which makes it an excellent choice for high power Li-ion battery applications.

The results presented here confirm that only minor changes are occurring in the layered structure of the cathode during Li insertion and removal ($0.29 \leq x \leq 0.78$). The bond lengths vary systematically in response to the change in the metal center's oxidation state. The short-range order in the mixed Ni/Co oxide layered system exhibits good reversibility during Li insertion/removal. Fitting the Ni-O bond to only one path results in a linear change in distance with the cathode state of charge. However, the overall change from fully discharged to fully

charged is greater than the change in the Co-O bond length. This observation, taken together with changes in the Debye-Waller factor, suggests that there is a second, longer Ni-O path in the discharged state (higher x). Finally, the charge compensation mechanism is different for the cobalt atoms compared with the nickel atoms near the top of charge. From the second-shell results, the Co appears to be oxidized by x = 0.47.

ACKNOWLEDGMENTS

This research was sponsored by the U.S. Department of Energy, Office of Basic Energy Science/Division of Chemical Science's Electrochemical Energy Storage and Conversion Program. Use of the Advanced Photon Source was supported by the U.S. Department of Energy, Basic Energy Sciences, Office of Science (DOE-BES-SC), under Contract No. W-31-109-Eng-38. The MRCAT is funded by the member institutions and DOE-BES-SC under contracts DE-FG02-94ER45525 and DE-FG02-96ER45589.

REFERENCES

[1] J.N. Riemers and J.R. Dahn, J. Electrochem. Soc. **139**, 2091 (1992).

[2] Y. Saadoune and C. Delmas, J. Mater. Chem. **6**, 193 (1996).

[3] S. Kostov, Y. Wang, M. L. denBoer, S. Greenbaum, C. C. Chang, and P. N. Kumpta, Mat. Res. Soc. Symp. Proc. **496**, 427-434 (1998).

[4] I. J. Pickering, G. N. George, J. T. Lewandowski, and A. J. Jacobson, J. Am. Chem. Soc. **115**, 4137-4144 (1993).

[5] I. Nakai and T. Nakagome, Electrochemical and Solid-State Letters **1** (6), 259-261 (1998).

[6] A. N. Mansour, J. McBreen, and C. A. Melendres, J. Electrochem. Soc. **146** (8), 2799-2809 (1999).

[7] W. E. O'Grady, K. I. Pandya, K. E. Swider, and D. A. Corrigan, J. Electrochem. Soc. **142**, 1613-1616 (1996).

[8] X. Sun, Q. Yang, J. McBreen, Y. Gao, M. V. Yakovleva, X. K. Xing, and M. L. Daroux, submitted to 1999 Joint International Meeting of the Electrochemical Society and the Electrochemical Society of Japan (1999).

[9] A. Rougier, C. Delmas, and A. V. Chadwick, Solid State Comm. **94** (2), 123-127 (1995).

[10] The electrolyte was 1 *M* $LiPF_6$ dissolved in 50 vol. % ethylene carbonate (EC) and 50 vol. % dimethyl carbonate (DMC) obtained as a solution from Merck Company.

[11] S. I. Zabinsky, J. J. Rehr, A. Ankudinov, R. C. Albers, and M. J. Eller, Phys. Rev. B **52**, 2995 (1995).

[12] E. A. Stern, M. Newville, B. Ravel, Y. Yacoby, and D. Haskel, Physica B **208&209**, 117 (1995).